UHF Radar Detection and Numerical Simulation of an Episode of Foehn and Lee Waves over the Northern Coast of Iberia

GOTZON GANGOITI,* LUCIO ALONSO, MERCEDES MARURI, AND MARINO NAVAZO

School of Industrial and Telecommunication Engineering, Universidad del Pais Vasco-Euskal Herriko Universitatea, Bilbao, Spain

GORKA PÉREZ-LANDA

Fundación CEAM, Paterna, Valencia, Spain

(Manuscript received 5 April 2001, in final form 27 August 2001)

ABSTRACT

This work shows an episode of foehn- and lee-wave activity over the sea-facing slopes of the Cantabrian Mountain Range, on the northern coast of Iberia, as detected by a wind profiler radar (WPR—LAP 3000 at 1290 MHz) at Punta Galea-Bilbao. Surface meteorological data from the regional network operated by the Basque Meteorological Service and the National Oceanic and Atmospheric Administration (NOAA) satellite images were also used to document the atmospheric dynamics. The period analyzed—17–18 January 1997—is included within the 1997 European Cooperation in the Field of Scientific and Technical Research (COST) Wind Initiative for a Network Demonstration in Europe (CWINDE-97) project, during which two well-defined severe wind episodes were registered over the Bilbao area as a result of consecutive frontal passages over the northern coast of Iberia. The results of a mesoscale model, running with nested grids down to a resolution of 3 km × 3 km, were used to understand the output of the profiler. Vertical winds at the WPR site showed a simultaneous pattern of upward and downward motion in the lower and upper layers, respectively, which was in accordance with the output of the model. The lee waves simulated by the high-resolution grid over the WPR site have been shown to be responsible for this pattern of vertical wind velocities. The vertical spatial distribution of dry and moist air, suggested by the signal-to-noise ratio of the radar, showed a ''reversed'' pattern of relative humidity distribution in the lower troposphere (higher values at upper levels) coincident with the foehn episode. The lee waves and the dry- and moist-air vertical distribution, which are associated with the strong southwesterly winds preceding the frontal systems over the coastal area, have been found to be responsible for range aliasing in the WPR lower-pulse mode.

1. Introduction

Frontal systems crossing the northern coast of Iberia from west to east have been observed to affect the performance of the wind profiler radar (WPR) placed on the north-facing slopes of the Cantabrian Mountain Range (Alonso et al. 1998; Maruri et al. 2000). The presence of nonuniform rain and sharp variations in the vertical distribution of the relative humidity are frequent during this type of episode. The main objective of the present manuscript is to analyze an episode of strong frontal activity over northern Iberia by using available local and synoptic data together with a mesoscale model output to explain the performance of the profiler.

The Regional Atmospheric Modeling System (RAMS version 3b; Pielke et al. 1992) was used first to evaluate its ability to simulate the observed local weather and then to help to understand the relative importance of the processes involved. The period analyzed in this paper is included within the 1997 European Cooperation in the Field of Scientific and Technical Research (COST) Wind Initiative for a Network Demonstration in Europe (CWINDE-97) project described by Oakley et al. (2000) and initiated by the European COST-76 Action. This cooperation program has been described by Monna (2000) and was supported by the European Commission. Numerous case studies were identified from the campaign period (January–February 1997), and the data archive at the Remote Sensing Branch of the Met Office (the CWINDE project office) was associated with the Fronts and Atlantic Storm-Track Experiment (FASTEX) campaign.

This paper is organized as follows: section 2 provides the area description, which is a key point to understanding the interactions between the frontal systems and the

* Current affiliation: Fundación CEAM, Paterna, Valencia, Spain.

Corresponding author address: Dr. Gotzon Gangoiti, Fundación CEAM, Parque Tecnológico, C/ Charles Darwin, 14. E-46980 Paterna, Valencia, Spain.
E-mail: gotzon@ceam.es

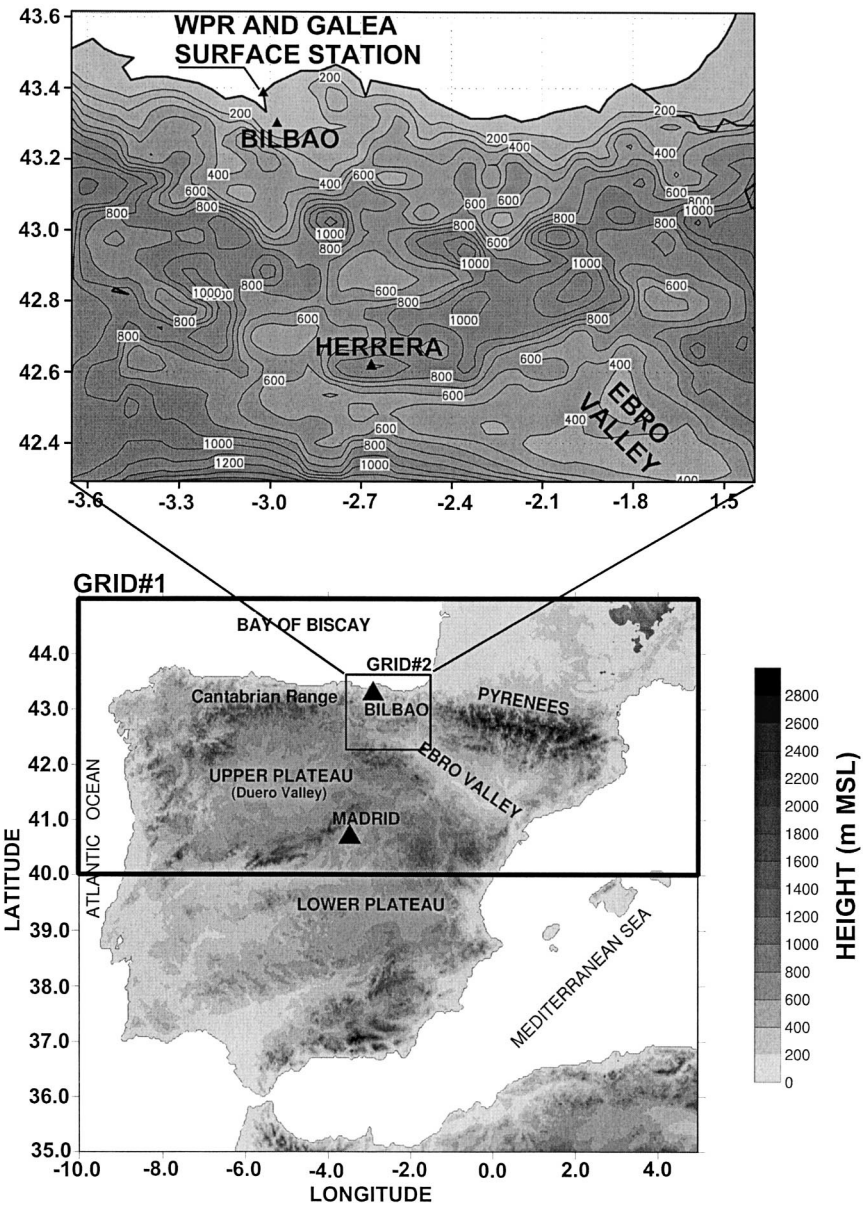

FIG. 1. (bottom) Lat–long topographic map of the Iberian Peninsula showing major topographic features and the coverage of the two nested grids used by the mesoscale model. (top) The location of the WPR and the two selected surface meteorological stations (Herrera and Galea) are also represented in the enlarged rectangle.

underlying terrain. The main meteorological equipment and its response are also described in this section. Experimental and modeling results are presented in section 3, and the paper concludes in section 4.

2. Meteorological equipment and area description

The topography of the Basque country is characterized by the presence of steep mountains (from sea level to a height of 1500 m), deep valleys, and a large coastal zone, which adds land–sea interactions to the local weather. The area can be completely enclosed within a 150 km × 150 km square, and it is located on the eastern side of the Cantabrian Mountain Range (enlarged square in Fig. 1), which extends along the north coast of the Iberian Peninsula and joins with the Pyrenees. The profiler is situated at the top of a 60-m-high cliff directly over the sea. This site (43.37°N, 3.01°W) is on the right bank of an estuary that runs nearly 16 km from Bilbao to the coast, aligned in a SE–NW direction.

The main characteristics of the WPR at Punta Galea

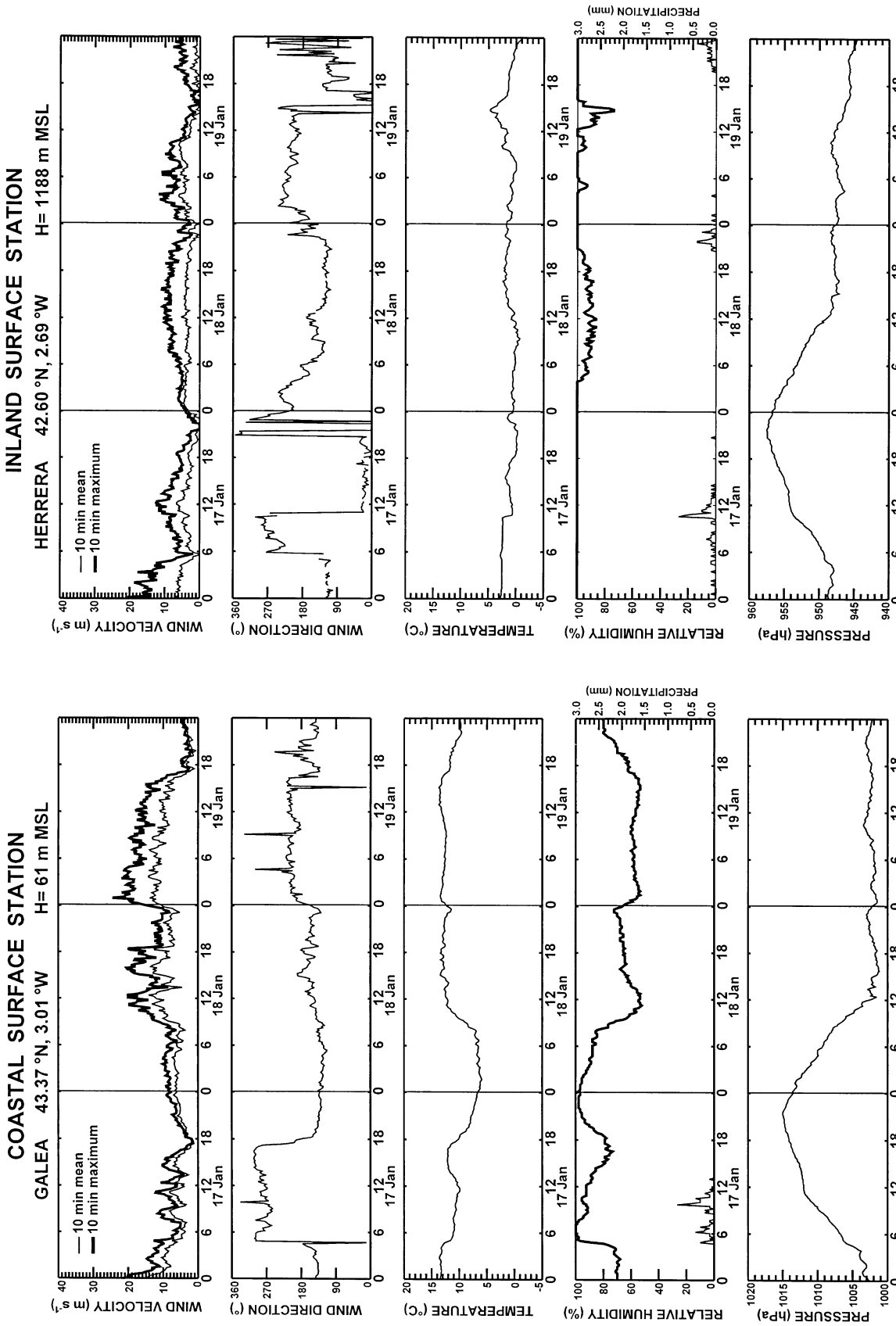

FIG. 2. Sequence of surface meteorological data at (left) a coastal and (right) an inland station (see Fig. 1). Longitude, latitude, and height of sites are shown on top. Three days of data are shown. The Herrera station does not record pressure data. Thus, the pressure time series of a nearby station located at 42.859°N, 2.688°W, and 546 m MSL is represented.

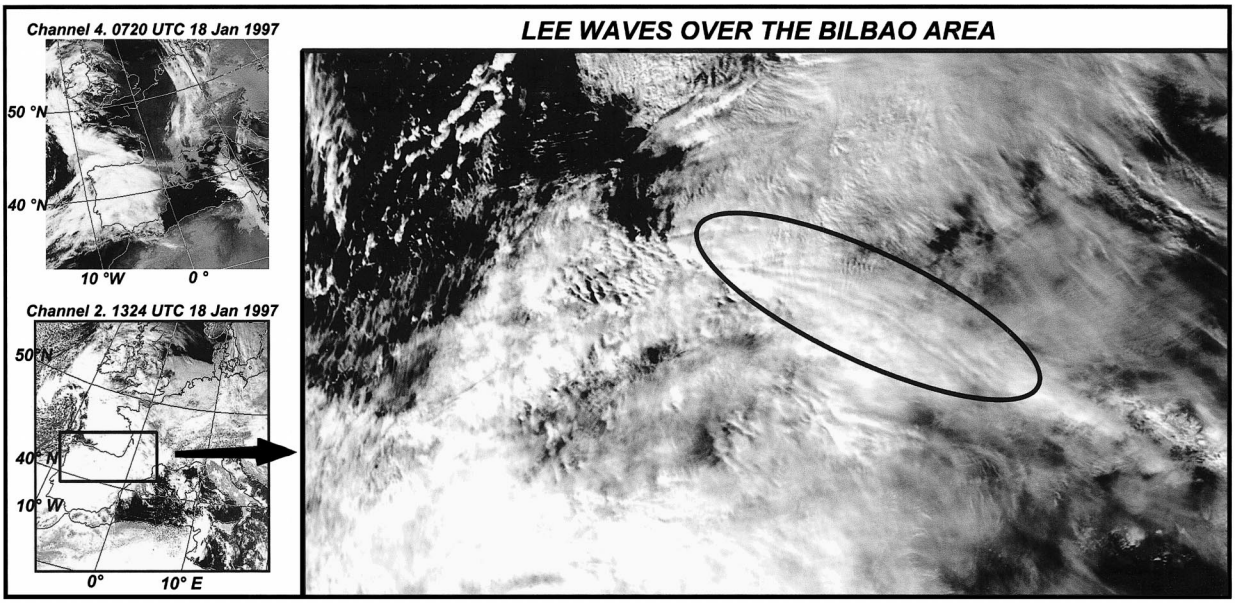

FIG. 3. NOAA image, on the visible wavelength of channel 2, illustrating the front associated with the cyclone NW of the Iberian Peninsula. The enlarged area shows the lee waves detected by the WPR. The image of a previous satellite pass at 0720 UTC, coincident with the cloud arrival over the WPR, is also shown (upper-left corner).

have been described in detail by Alonso et al. (1998). The system (LAP 3000 at 1290 MHz) utilizes nine antenna panels; its operation during the selected episode included signal processing on five beams and two pulse widths (100- and 400-m vertical resolutions, which correspond to the short- and long-pulse modes). Twenty-five-minute wind averages were obtained for both resolutions, and 5-min virtual temperatures for the higher resolution. Profilers operating in the UHF range are sensitive to the backscattered power from structures at one-half the operating wavelength because of gradients of the refractive index in the atmosphere (known as Bragg scattering) as well as to small point targets in the profiler pulse volume (known as Rayleigh scattering). The performance of the profilers depends on atmospheric conditions (Radian 1995): temperature and humidity variations carried by the turbulence are responsible for the fluctuations in the refractive index of the atmosphere, while Rayleigh scattering in clouds and hydrometeors is also registered whenever these conditions are present over the profiler. In 1996, a field campaign with radiosondes, performed under different meteorological conditions, demonstrated that measures obtained by the WPR at Punta Galea were within the limits defined by the manufacturer (Alonso et al. 1998).

In addition, 10-min averages of temperature, pressure, humidity, radiation, precipitation, and wind, recorded by a dense network of 60 surface stations distributed over the area, contributed to the evaluation of the local weather and the model response during the frontal episode.

3. Results

a. Synoptic weather pattern and surface meteorological observations

Two fast-moving frontal systems, separated by 36 h, crossed the northern coast of the Iberian Peninsula on 17 and 18 January 1997, causing an intense wind episode. Although no serious damage was reported at the time, the synoptic weather maps confirmed a potential danger due to the distribution and relative strength of the pressure systems approaching the Iberian Peninsula. West-to-east-moving fronts push moist Atlantic air masses towards the west coast of the peninsula. Then, they ascend to the upper plateau, condense, and precipitate on the sea-facing slopes of the mountains near the west and northwest coast of Iberia (Fig. 1). In the meantime, the warm sector of the front system pushes south-to-southwesterly winds toward the northern coast. Thus, upslope condensation and precipitation are also frequent on the south-facing slopes of the Cantabrian Range. Southwesterly winds over the Cantabrian Range bring dry and relatively high temperatures on the northern coastal locations as a result of a sharp foehn wind. The western Iberian coast and the south and southwesterly facing slopes of the Iberian upper and lower plateau registered important amounts of precipitation during 18 January, while the northern coast kept dry and relatively warm (a temperature difference of 5–6°C was registered between the surface stations at the northern coast and at the upper plateau, which has an average height of 600 m MSL. This is the type of flow pattern we found during the first 4 h of 17 January and the late morning

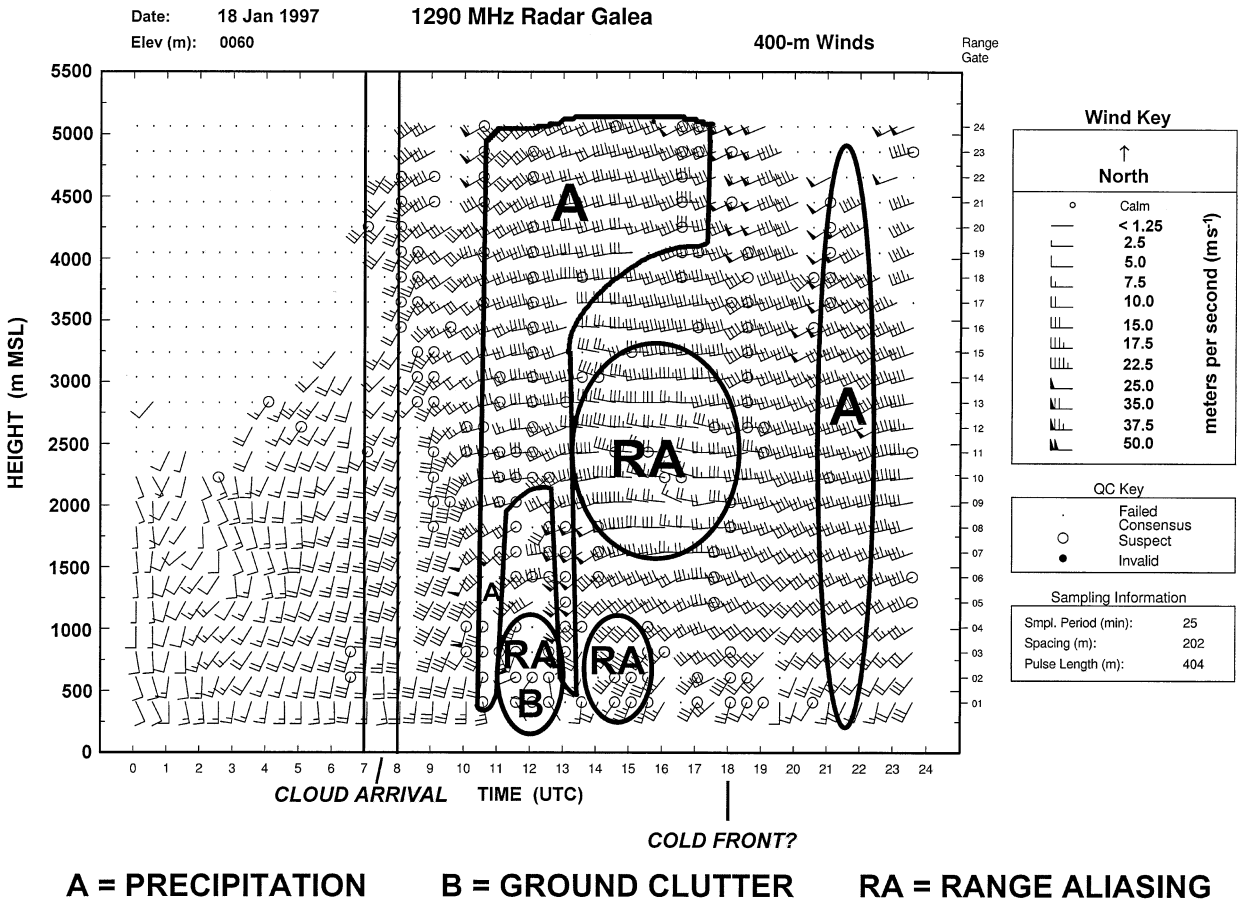

FIG. 4. Sequence of wind profiles of the radar for the longer pulse during the second frontal episode (18 Jan 1997). Cold front was not clearly detected at the coastal surface stations.

and afternoon of 18 January (Fig. 2), corresponding to both prefrontal episodes. Some of the maxima registered in the wind records of the Basque country were coincident with a marked southwesterly direction. The passage of a cold front is indicated when there is a simultaneous drop in temperature and an increase in relative humidity, rain, and wind veering, normally to the west-northwest; but this wind veering is conditioned by channeling and other topographical effects: see the pattern of surface meteorological data shown in Fig. 2 at 0400 UTC 17 January 1997. However, the passage of the second cold front during the late evening of 18 January was detected at the inland surface stations (Iberian upper plateau) but it was not observed at the coastal stations of the Bilbao area. This is a clear example of the influence of the topography in the modification of the properties of air masses at a local scale. Warming of the lower layers and a corresponding decrease in relative humidity over the coastal area due to the foehn is the cause of the observed differences between coastal and inland stations during the evening of 18 January: no rain was detected at any of the coastal surface stations during this day, while at the inland stations almost all the rain gauges detected precipitation during the late evening and nighttime period (see inland station of Fig. 2). Temperature rises registered at ≈0800 UTC 18 January at the coastal stations (within the warm sector of the second front system) were kept high throughout the rest of the day, with simultaneous low values of the RH. The National Meteorological Services included a cold front in their forecasting and analysis charts, which, at 1800 UTC 18 January, was located over the Bilbao area and, 6 h later, had already crossed the area and was located at western France. The coastal stations recorded a wind maximum coincident with the expected cold front passage at 1800 UTC 18 January, and the WPR observed a high-level jet, as described in the next section.

Figure 3 shows two consecutive National Oceanic and Atmospheric Administration (NOAA) images of the frontal passage during 18 January. The infrared image of channel 4 (10.5–11.5 μm) is coincident with the arrival of the higher clouds over the eastern Bay of Biscay. The visible image of channel 2 (0.725–1.10 μm) corresponds to the next satellite pass and shows high- and middle-level clouds over the Bilbao area, still in the

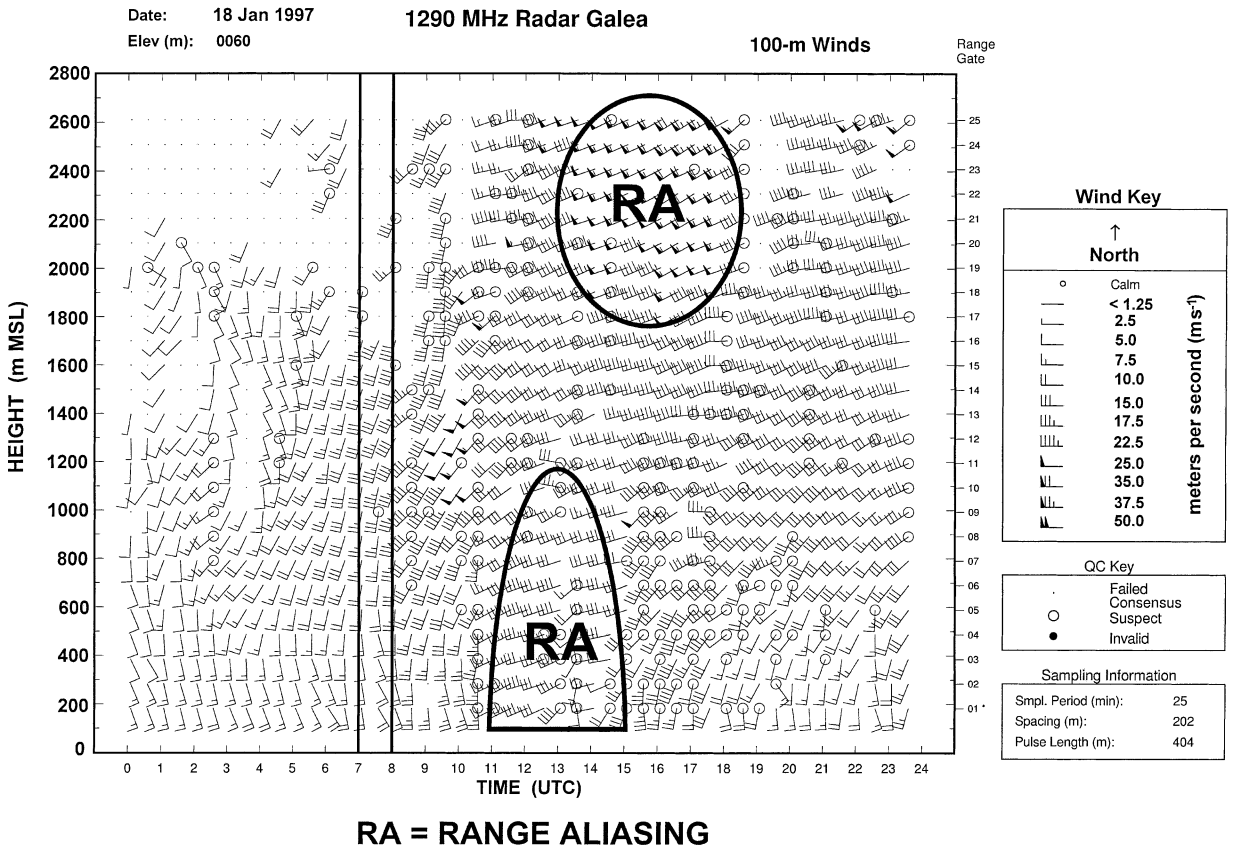

FIG. 5. Sequence of wind profiles of the radar for the short-pulse mode during the second frontal episode (long-pulse output shown in Fig. 4). Winds in regions marked RA are erroneously estimated in the short-pulse mode.

warm sector of the frontal system. The enlarged area of the visible image shows lee waves over the coast and the easternmost edge of the Cantabrian Range. Their wavelength is between 14 and 16 km (enlarged area in Fig. 3).

b. WPR observations

The refractive index at microwave frequency depends mainly on temperature and humidity as described in section 2. Therefore, there is a close link between refractive index—temperature and humidity—fluctuations carried by the atmospheric wind and turbulence, and the return power. Vertical variations in a computed refractive index from radiosonde measurements of temperature and humidity have been shown to correlate well with variations in the signal-to-noise ratio (SNR) of ultra high frequency (UHF) profilers (Gaffard and Nash 2000); dry and stable air masses (e.g., under a sinking process) are expected to show a reduced SNR. Figure 4 shows the time sequence of wind profiles for the longer-pulse mode of the WPR. The limited vertical coverage (2500–3000 m MSL) of the WPR observed in Fig. 4, from 0000 to 0700 UTC, can be associated with the sinking (stabilization) and drying of the air mass behind the first cold front passage on 17 January. After that period, the high-mode wind vectors depicted in the figure show increasing vertical coverage, coincident with cloud arrival in the warm sector of the second frontal system (marked with two solid lines between 0700 and 0800 UTC). A simultaneous increase in wind speed was observed at all levels: wind maxima were registered above 4000 m between 1800 and 2100 UTC, coincident with the cold front passage detected at the inland surface stations (Fig. 2). The arrival of clouds over the profiler was estimated using weather satellite images (Fig. 3) and visual observations at the main weather stations of the National Weather Services located at northern Iberia and southern France. These observations were part of the analysis available every 3 h in the U.K. Meteorological Service during the CWINDE project.

Areas marked A and B in Fig. 4 correspond to precipitation periods and ground clutter, respectively. Areas marked RA in Figs. 4 and 5 show short transitory periods of range-aliasing artifacts: echoes from different pulses in the same time interval (Doviak and Zrnić 1993), detected in the high-resolution mode during the quality control process (checking for consistency between modes). These conditions appear with high SNR

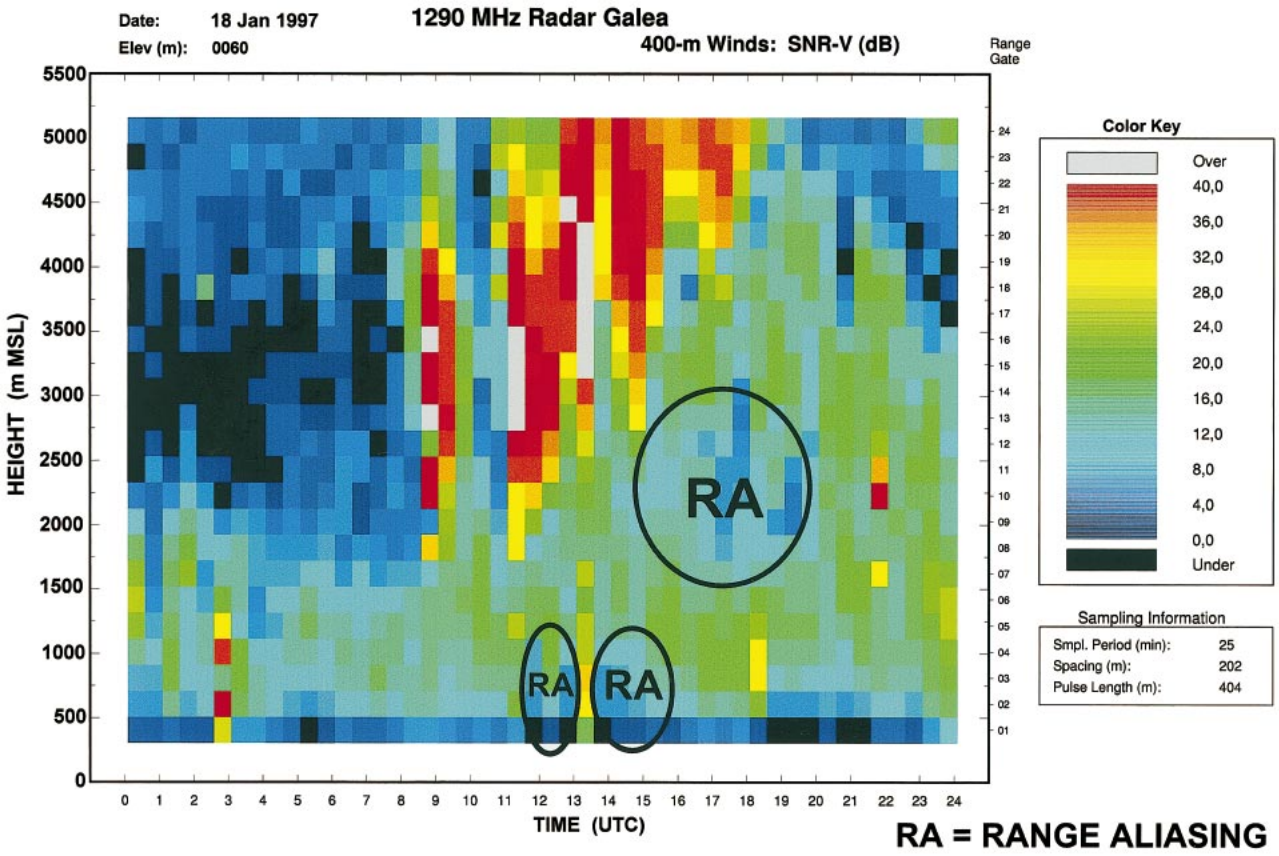

FIG. 6. Sequence of the SNR for the vertical beam (long-pulse mode) of the WPR.

in the upper levels, due to enhanced backscattering by clouds and hydrometeors, together with a relatively low SNR at lower heights due to a weaker backscattering by drier air layers located near the surface (Fig. 6): the reversed lower-to-midtroposphere distribution of relative humidity at the coastal site during the second half of the day is associated with a foehn on the lee side of the Cantabrian Range. Vertical wind detected by the profiler (Fig. 7) shows a ''coherent'' pattern of upward-moving air for the lower layers (in green–yellow) and simultaneous downward movements for the upper layers (in blue) after midday from 1600 to 1930 UTC. The mesoscale model simulation described in the next section will help to explain the observed dynamics during this time interval.

The effect of precipitation on UHF wind profiler measurements and the reliability of this type of radars to retrieve horizontal winds have been evaluated by different authors (see, e.g., Wuertz et al. 1988). However, during frontal episodes, such as the one described here, the simultaneous presence of horizontally and vertically nonhomogeneous rain during the consensus averaging period poses some difficulties to the algorithms of the real data-processing chain in the assignment of the vertical wind to an atmospheric layer (Maruri et al. 2000). From 1100 to 1500 UTC most of the vertical profiles and range gates show nonhomogeneous rain (highest values of the SNR in Fig. 6—red and yellow—and highest values for the downward velocities—dark blue and black—in Fig. 7) and clutter, and as a consequence, they will not be used to compare with the mesoscale model results described in the next section.

Vertical wind velocities above 2500–3000 m between 0000 and 0800 UTC and above 3500–4000 m between 2000 and 2400 UTC are not valid because of a very low SNR. Thus, they will also be excluded from being compared with the mesoscale model results.

c. Numerical model results

The RAMS model was used to carry out the simulation. It is a nonhydrostatic prognostic model and was initialized using National Centers for Environmental Prediction (NCEP) reanalysis data, with a resolution of 2.5° × 2.5°. Two nested grids were used (grid 1 and grid 2 in Fig. 1), with 12 km × 12 km and 3 km × 3 km resolution on the horizontal dimension and variable resolution on the vertical, from 0 to 12 000 m in height, with minimum increases of 25–100 m close to the ground and maxima of 1000 m at the higher levels. A total of 34 levels were included for both resolutions. Two-way nesting was allowed between the grids, so that

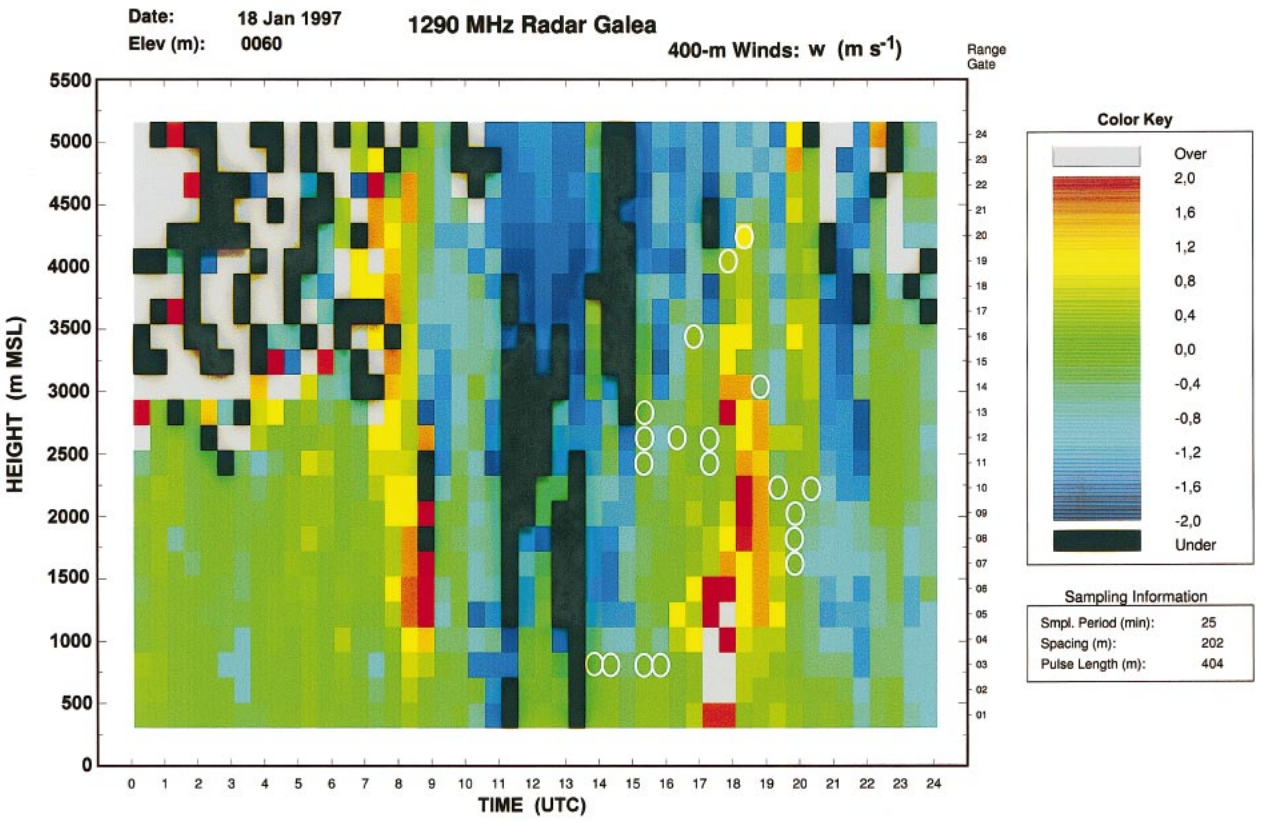

FIG. 7. Sequence of vertical wind profiles of the radar for the long-pulse mode. Simultaneous upward (lower layers) and downward (upper layers) airflows are observed between 1600 and 1930 UTC: zero velocity range gates are marked with open white circles to show the transitions from positive to negative values of the vertical velocity.

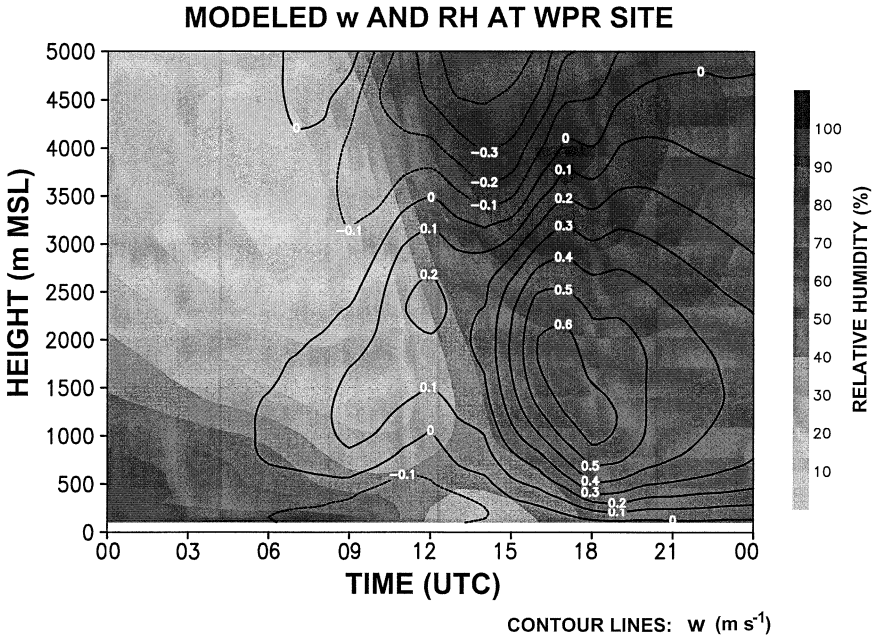

FIG. 8. Simulated relative humidity (shaded) and vertical velocities (contour lines) vs height (m MSL) for 18 Jan 1997.

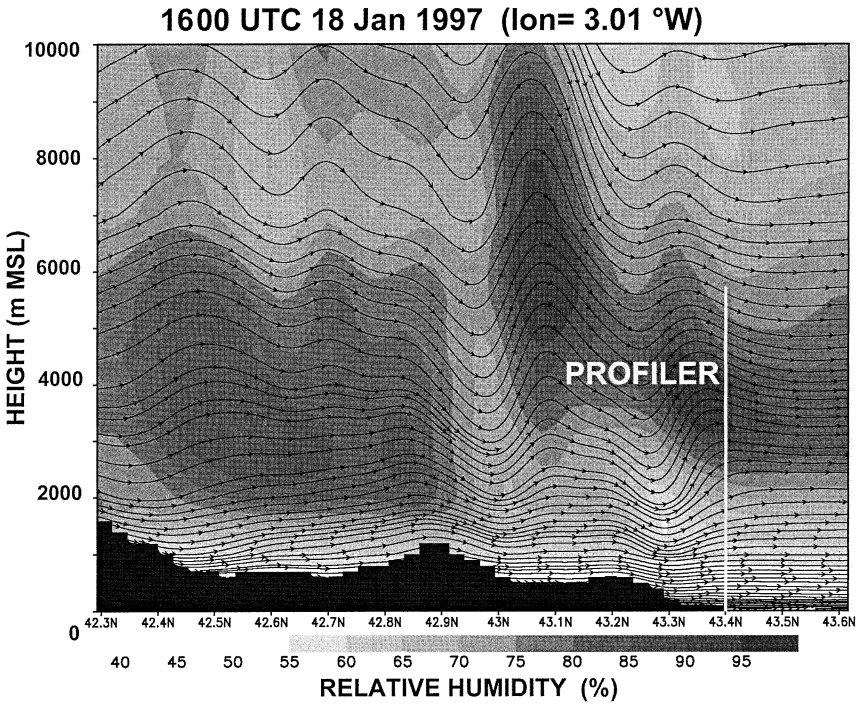

FIG. 9. Simulated streamlines and relative humidity at a longitudinal cross section of the finer grid of the model. The selected longitude is that of the WPR site.

the finer grid conditioned the flow in the coarser grid and vice versa. The four-dimensional data assimilation technique was used for the running, nudging the boundary of the grids to the conditions established by the NCEP reanalysis data at 0000, 0600, 1200, and 1800 UTC. The run extended over 17, 18, and 19 January 1997. The fine grid included the whole Basque country (enlarged rectangle in Fig. 1), while the coarse grid covered the northern coast of the Iberian Peninsula plus the southern region of France. Topography was interpolated to the model grid from the global 30″ latitude–longitude database. Land use was obtained from the original Fifth-Generation Pennsylvania State University–National Center for Atmospheric Research (NCAR) Mesoscale Model (MM5) database, with a resolution of 5′ (Grell et al. 1994). Sea surface temperature was interpolated from the along-track scanning radiometer (ATSR) monthly-averaged satellite data, with a latitudinal–longitudinal resolution of 0.5° (Edwards et al. 1990).

Comparison of the modeled wind with the WPR output showed relatively good agreement, except for periods related to rapid wind veering at the exact time of the frontal passage over the WPR. Differences in the horizontal wind intensity between profiler and model estimations were found to be within a range of 30% of the WPR wind measurements (Gangoiti 1998). This agreement gave us enough confidence to undertake further comparisons. Figure 8 represents the temporal sequence of the vertical wind and relative humidity profiles calculated by the RAMS model at the profiler for 18 January. The sequence of both variables shows a complete reversal from morning to afternoon conditions. The dry air with a slow downward motion registered in the upper levels during the morning is replaced by a moist air mass during the afternoon, while the moist air (80%–90% relative humidity) found in the lower layers (below 500 m) during the morning is replaced by drier air (40%–60%) during the afternoon. Thus, the profiles of humidity and vertical velocity turned upside-down during the transition from morning to afternoon, coincident with the approach of the second frontal system. The numerical simulation of the relative humidity in Fig. 8 is well correlated with the SNR of the radar (Fig. 6) and its vertical coverage (Figs. 4–7): during the morning of 18 January, very low values of relative humidity in the upper levels (Fig. 8), coincident with the sinking and stabilization of the air masses behind the first front system, result in a decrease in the vertical coverage of the WPR during this time period. Low relative humidity values in the lower layers, together with the scale of the turbulence associated with this type of wind during the second half of the day (Fig. 8), are also in good agreement with the low SNR values in the short-pulse return (not shown). The highest values of relative humidity after midday and above 2000–2500 m are coincident with the high SNR values observed in Fig. 6 at the corresponding levels: Rayleigh scattering in the clouds containing rain, snow, or other large hydrome-

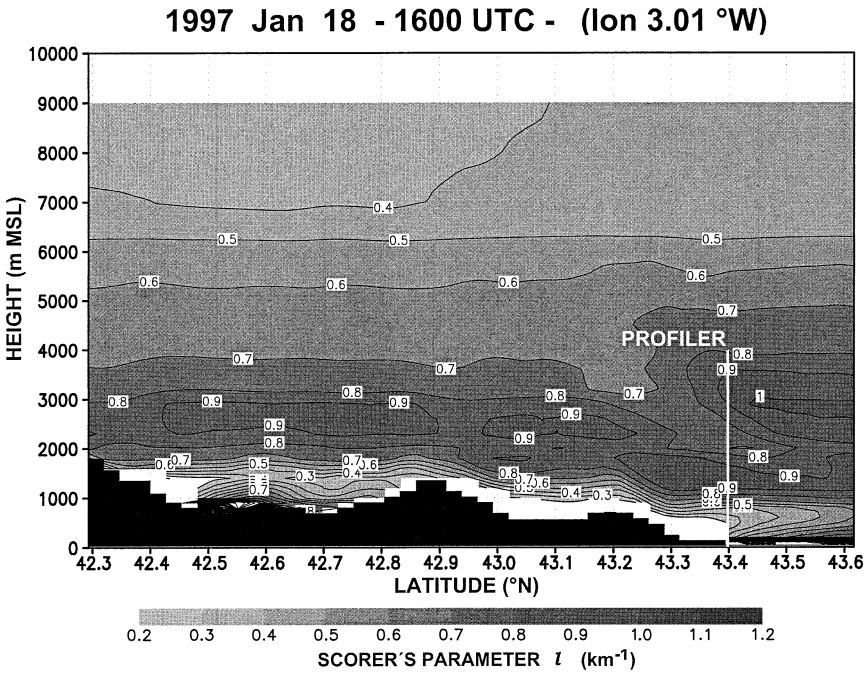

FIG. 10. Scorer's parameter at the same longitudinal cross section and time shown in Fig. 9.

teors is responsible for the high SNR values detected in the upper levels with the long-pulse mode.

The behavior of the vertical wind velocity at the profiler (Fig. 7) is similar to that observed in the model (Fig. 8) during the afternoon–evening period when there is a good SNR and when there is no precipitation observed in most of the range gates. At that time interval (1600–1930 UTC) the profiler detects a strong upward motion of dry air for the lower levels and a simultaneous downward motion for the upper levels. The model was able to capture this complex behavior. In order to understand the type of air dynamics leading to these profiles of humidity and vertical velocity, a longitudinal cut of the finer grid at 1600 UTC and at the longitude of the profiler site (3.01°W) is represented in Fig. 9. Relative humidity and streamlines obtained with the v and $10 \times w$ components of the wind show mountain lee waves that cross the profiler site at latitude 43.37°N (white vertical line in Fig. 9). The lower and upper waves show a phase displacement in the model output, which results in the simultaneous upward and downward motion detected by the WPR for every profile between 1600 and 1930 UTC. After 1100 UTC, the mesoscale model generates lee waves over the WPR site. NOAA satellite images show waves of approximately the same amplitude as those depicted in Fig. 9. However, the precipitation observed at the middle and high range gates of the WPR between 1100 and 1500 UTC prevents an adequate comparison of the WPR data and the model output at the exact time of the satellite pass.

In Fig. 9 there are trapped low-level lee waves as well as vertically propagating waves aloft with tilted phase lines. Trapped lee-wave development is favored when there is an increase in wind velocity and/or a decrease in stability with height (Scorer 1997). These criteria imply a decrease with height of l^2, where l is Scorer's parameter. Neglecting effects due to large shear in the vertical wind profile and curvature terms, l^2 can be estimated by using the Boussinesq form of Scorer's parameter (Barry 1992):

$$l^2 = \frac{g}{U^2}\left(\frac{1}{\theta}\frac{\partial\theta}{\partial z}\right),$$

where U is the wind velocity perpendicular to the barrier (m s^{-1}), g is the gravitational acceleration (m s^{-2}), and θ is the potential temperature (K).

Figure 10 represents l (km^{-1}) versus height, at the same instant and vertical cross section as that represented in Fig. 9. White areas over the terrain level correspond to the lowest values of Scorer's parameter. Large areas of decreasing l with height can be observed above 1200 m over the coast and above 2500 m over land: when l decreases rapidly with height, wave energy may be partially or totally reflected in that layer. Model results show partial reflection and a pattern of ''leaky trapped lee waves.''

4. Conclusions

Joint usage of a boundary layer WPR and a mesoscale model, applied with sufficient horizontal and vertical resolution, has enabled us to identify and diagnose an episode of wave activity and foehn on the lee side of

the Cantabrian Range on the northern coast of Iberia. During a foehn episode, the irruption of dry air in the lower coastal levels causes a transient sharp reduction in the SNR observed in the short-pulse (high resolution) mode. The simultaneous presence of clouds and hydrometeors aloft, detected by the WPR and confirmed by satellite images and model evaluations, gives rise to a high long-pulse SNR in the uppermost ranges, which, during these transient periods, interferes with the reception of the short-pulse return signal. Thus, frontal passages during periods of strong southwesterly winds over the area must be carefully screened by quality control procedures (checking mainly for consistency between modes) to correct for remaining range aliasing artifacts not detected in the real-time data processing chain.

The vertical wind velocity distribution over the profiler shows a pattern of simultaneous upward and downward motion for the upper and lower layers during this type of frontal episode. At the same time, the mesoscale model results show the presence of lee waves with an upstream phase tilt with height. This wave pattern detected by the radar is far from being steady during the whole episode. It appears and disappears abruptly after a few hours and is concurrent with discontinuous and nonhomogeneous rain, posing an important challenge to WPR operation. Moreover, similar frontal episodes are frequent over this area because it is subject to continuous frontal passages all year except during the summer period.

Acknowledgments. This work has been partially supported by the Commission of the European Communities, under the COST-76 action. The University of the Basque Country and the Basque Service of Meteorology also supported this work. The Fundación CEAM, which also contributed to the present work, is financed by the Generalitat Valenciana and Bancaixa. Last, we acknowledge the U.S. National Weather Service for providing the reanalysis data.

REFERENCES

Alonso, L., G. Gangoiti, M. Navazo, M. Maruri, J. A. García, and J. A. Aranda, 1998: The Punta Galea boundary layer profiler: Intercomparison with radiosonde data and first mesoscale meteorological case studies. *Meteor. Z.*, N.F.7(H.5), 203–212.

Barry, R. G., 1992: *Mountain Weather and Climate.* Routledge Physical Environment Series, 402 pp.

Doviak, R. J., and D. S. Zrnić, 1993: *Doppler Radar and Weather Observations.* Academic Press, 562 pp.

Edwards, T., and Coauthors, 1990: The along track scanning radiometer measurement of sea-surface temperature from ERS-1. *J. Br. Interplanet. Soc.*, **43,** 160–180.

Gaffard, C., and J. Nash, 2000: Initial evaluation of signal power characteristic of a boundary layer profiler in the UK. *Proc. Ninth International Workshop on Technical and Scientific Aspects of MST Radar Combined with COST-76 Final Profiler Workshop,* Toulouse, France, SCOSTEP and Météo France, 431–434.

Gangoiti, G., 1998: Assessment of the Bilbao wind profiler data during the CWINDE-97 campaign in the framework of an experimental European windprofiler network, STSM report, March 1998. COST-76 Working Doc. 76/Doc/57, 21 pp.

Grell, G. A., J. Dudhia, and D. R. Stauffer, 1994: A description of the fifth generation Penn State/NCAR mesoscale model (MM5). NCAR Technical Note, NCAR/TN-398+STR, 122 pp.

Maruri, M., M. Matabuena, G. Gangoiti, M. Navazo, and L. Alonso, 2000: Analysis of spectral data for enhanced data recovery and quality control in a BLP at a coastal site. *Proc. Ninth International Workshop on Technical and Scientific Aspects of MST Radar Combined with COST-76 Final Profiler Workshop,* Toulouse, France, SCOSTEP and Météo France, 475–479.

Monna, W. A., 2000: COST-76, aims, achievements and future. *Proc. Ninth International Workshop on Technical and Scientific Aspects of MST Radar Combined with COST-76 Final Profiler Workshop.* Toulouse, France, SCOSTEP and Météo France, ix–xii.

Oakley, T., J. Nash, and M. Turp, 2000: CWINDE project office networking of European profilers 1997–2000. *Proc. Ninth International Workshop on Technical and Scientific Aspects of MST Radar Combined with COST-76 Final Profiler Workshop,* Toulouse, France, SCOSTEP and Météo France, 525–528.

Pielke, R. A., and Coauthors, 1992: A comprehensive meteorological modeling system—RAMS. *Meteor. Atmos. Phys.*, **49,** 69–91.

Radian Corporation, 1995: Training guide for the LAP®-3000. Doc. Control 80018502, Revised 1.0. Radian Corporation, Electronics Division, 62 pp.

Scorer, R. S., 1997: *Dynamics of Meteorology and Climate.* John Wiley and Sons, 686 pp.

Wuertz, D. B., B. L. Weber, R. G. Strauch, A. S. Frisch, C. G. Little, D. A. Merrit, K. P. Moran, and D. C. Welsh, 1988: Effects of precipitation on UHF wind profiler measurements. *J. Atmos. Oceanic Technol.,* **5,** 450–465.